1-2018

Constitutive MAP-kinase Activation Suppresses Germline Apoptosis in NTH-1 DNA Glycosylase Deficient *C. elegans*

Henok Kassahun
University of Oslo

Tamina SenGupta
University of Oslo

Alfonso Schiavi
Leibniz Research Institute for Environmental Medicine

Suzanne Estes
Portland State University

Silvia Maglioni
Leibniz Research Institute for Environmental Medicine

See next page for additional authors

Citation Details

Kassahun, H., SenGupta, T., Schiavi, A., Maglioni, S., Skjeldam, H. K., Arczewska, K., ... & Nilsen, H. (2018). Constitutive MAP-kinase activation suppresses germline apoptosis in NTH-1 DNA glycosylase deficient C. elegans. DNA repair, 61, 46-55.

DNA Repair 61 (2018) 46–55

Contents lists available at ScienceDirect

DNA Repair

journal homepage: www.elsevier.com/locate/dnarepair

Constitutive MAP-kinase activation suppresses germline apoptosis in NTH-1 DNA glycosylase deficient *C. elegans*

Henok Kassahun[a,1], Tanima SenGupta[a,1], Alfonso Schiavi[b], Silvia Maglioni[b], Hanne K. Skjeldam[a,f], Katarzyna Arczewska[a,e], Nicole L. Brockway[c], Suzanne Estes[c], Lars Eide[d], Natascia Ventura[b], Hilde Nilsen[a,*]

[a] *Institute of Clinical Medicine, Department of Clinical Molecular Biology, University of Oslo and Akershus University Hospital, Lørenskog, Norway*
[b] *Institute of Clinical Chemistry and Laboratory Medicine of the Heinrich Heine University, and the IUF – Leibniz Research Institute for Environmental Medicine, Auf'm Hennekamp 5040225 Duesseldorf, Germany*
[c] *Portland State University, Department of Biology, Portland, OR, United States*
[d] *Department of Medical Biochemistry, University of Oslo and Oslo University Hospital, Norway*
[e] *Centre of Postgraduate Medical Education, Department of Biochemistry and Molecular Biology, Warsaw, Poland*
[f] *Novartis, Nydalen Allé 37 A 0484 Oslo, Norway*

ARTICLE INFO

Keywords:
C. elegans
Base excision repair
NTH-1
Apoptosis
Oxidative stress

ABSTRACT

Oxidation of DNA bases, an inevitable consequence of oxidative stress, requires the base excision repair (BER) pathway for repair. *Caenorhabditis elegans* is a well-established model to study phenotypic consequences and cellular responses to oxidative stress. To better understand how BER affects phenotypes associated with oxidative stress, we characterised the *C. elegans nth-1* mutant, which lack the only DNA glycosylase dedicated to repair of oxidative DNA base damage, the NTH-1 DNA glycosylase.

We show that *nth-1* mutants have mitochondrial dysfunction characterised by lower mitochondrial DNA copy number, reduced mitochondrial membrane potential, and increased steady-state levels of reactive oxygen species. Consistently, *nth-1* mutants express markers of chronic oxidative stress with high basal phosphorylation of MAP-kinases (MAPK) but further activation of MAPK in response to the superoxide generator paraquat is attenuated. Surprisingly, *nth-1* mutants also failed to induce apoptosis in response to paraquat. The ability to induce apoptosis in response to paraquat was regained when basal MAPK activation was restored to wild type levels. In conclusion, the failure of *nth-1* mutants to induce apoptosis in response to paraquat is not a direct effect of the DNA repair deficiency but an indirect consequence of the compensatory cellular stress response that includes MAPK activation.

1. Introduction

Base Excision Repair (BER) is an evolutionarily conserved pathway that removes a wide range of modified DNA bases. BER is the most important pathway for repair of oxidised DNA bases, an inevitable consequence of oxidative stress. As oxidative stress is known to accompany aging and a wide range of human age-related diseases, it can be expected that BER would be important for maintaining health during aging. This, however, has been difficult to firmly demonstrate. Lesion specificity in BER is provided by the initial step wherein modified bases are detected and excised by DNA glycosylases [1]. In mammalian cells, there are several DNA glycosylases that recognise and remove oxidised DNA bases. DNA glycosylases have overlapping substrate specificities, and the lack of adverse phenotypes of DNA-glycosylase deficient mouse models has been explained by extensive redundancy [2]. Thus, to further understand the role of BER in general, and DNA glycosylases in particular, in counteracting deleterious effects of oxidative stress, there is a need to study the consequence of BER defects in other animal models.

The nematode *Caenorhabditis elegans* is an established animal model for studies of oxidative stress and DNA damage responses [3]. Work in *C. elegans* also has the potential to uncover phenotypes associated with BER deficiency that may be masked in mammals due to extensive redundancy because the *C. elegans* genome encodes only two DNA glycosylases, UNG-1 [4–6] and NTH-1 [7]. Other *C. elegans* BER enzymes include two AP-endonucleases, EXO-3 [8] and APN-1 [9], of which

* Corresponding author.
E-mail address: hilde.nilsen@medisin.uio.no (H. Nilsen).
[1] These authors contributed equally to the work.

https://doi.org/10.1016/j.dnarep.2017.11.009
Received 14 September 2017; Received in revised form 24 November 2017; Accepted 28 November 2017
Available online 29 November 2017

EXO-3 is homologous to the mammalian APE1 enzyme [10]. There is no ortholog of DNA polymerase β but BER has been demonstrated in *C. elegans* [11] and likely utilizes DNA polymerase θ or a replicative DNA polymerase [12].

The endonuclease III homolog NTH-1 is the only representative of DNA glycosylases known to repair oxidative DNA base damage in *C. elegans*. Like its mammalian counterpart, NTH-1 has activity on a range of oxidised pyrimidines, like thymine glycol, 5-hydroxymethyluracil (5-hmU), and 5-formyluracil (5-foU), but also on 8-oxoG when base paired with G [7]. A null mutant, *nth-1(ok724)* which carries a deletion spanning exons 2 through 4 of the *nth-1* gene, showed normal mean and maximum lifespan [7,13], no hypersensitivity to the oxidizing agents H_2O_2 or paraquat but a mild sensitivity to juglone [13]. Previously, Hunter and co-workers [14] failed to observe any difference in *in vivo* repair of nuclear or mitochondrial DNA in *nth-1* mutants following treatment with H_2O_2. Loss of NTH-1 did, however, suppress the reproductive deficit of *exo-3* mutants [10], supporting that NTH-1 functions as a DNA glycosylase *in vivo* and generates AP-sites, which are substrates for EXO-3 in the germline.

Here, we show that *nth-1* mutants exhibit chronic oxidative stress and mitochondrial dysfunction and fail to mount an apoptotic response to the superoxide generator paraquat. The inability to induce apoptosis was not a direct consequence of the DNA repair defect. Instead, failure to induce germline apoptosis was a consequence of compensatory cellular stress response that includes elevated basal phosphorylation of the mitogen-associated stress activated kinase (MAPK) PMK-1 and JNK-1. These results show that phenotypes in DNA-repair mutants that could be interpreted as direct consequences of the repair defect may instead be indirect consequence of cytoprotective stress responses that compensate for DNA repair deficiency.

2. Materials and methods

2.1. Strains and culture conditions

All strains were maintained at 20 °C as described [15] unless otherwise stated. The reference strain Bristol N2 and RB877 *nth-1*(*ok724)III*, unc-58(e665)X, MD701 *($P_{lim\text{-}7}$ced-1:gfp),* and CL2166 [*dvIs19[pAF15(gst-4:gfp:NLS)]* III] [16] strains were kindly provided by the *Caenorhabditis* Genetic Centre (University of Minnesota, St Paul, MN, USA). All strains were backcrossed at least 6 times into the N2 strain. The RB877 strain is referred to as *nth*-1 in subsequent sections. The transgenic strains *nth-1*;*($P_{lim\text{-}7}$ced-1:gfp)* and *nth-1*;*unc-58* were generated for this work. *Escherichia coli* strains OP50 and HT115(DE3) for RNAi studies, and BK2118 (*tag alkA)* were used as food sources. For RNAi experiments, worms were maintained for one generation on Nematode Growth Medium (NGM) plates containing 2 mM IPTG (isopropyl b-D-1-thiogalactopyranoside) seeded with *Escherichia coli* HT115(DE3). All experiments were performed at 20 °C unless otherwise stated.

2.2. Chemicals and antibodies

Paraquat (PQ), methyl viologen dichloride hydrate, was purchased from Sigma. The following commercially available antibodies were used for immunofluorescence and western blotting: phosphorylated PMK-1 (T180/Y182) (Cell signalling D3F9), phosphorylated JNK-1(T183/Y185) (NOVUS NBP1-72242), phosphorylated H3 (Ser 10) (Santa Cruz Biotechnology Inc,) and actin (Abcam ab1801). The specificity of the antibodies detecting phosphorylated PMK-1 and JNK-1 were validated by immunostaining after RNAi mediated depletion of PMK-1 and JNK-1 (Supplementary Fig. S3). Secondary antibodies were Alexa Fluor® 488 conjugate anti-rabbit (Invitrogen), enhanced chemiluminescence (ECL) anti-rabbit IgG horseradish peroxidase (HRP)-linked whole antibody (Thermo Scientific), and anti-rabbit IgG HRP-linked (Santa Cruz).

2.3. DNA damage induced apoptosis

Synchronized [$P_{lim\text{-}7}$*ced-1:gfp*] and *nth-1*(*ok724*);[$P_{lim\text{-}7}$*ced-1:gfp*] L4 hermaphrodites were exposed to 400 μM paraquat on NGM plates, or 5 mM *N*-ethyl-*N*-nitrosourea (ENU) as a positive control. Germ-cell corpses were identified by the presence of a GFP outline around the cells undergoing apoptosis in the pachytene region 24 h post-treatment. The number of germ-cell corpses per gonad arm was scored under a Zeiss Axioplan microscope equipped with a 63xPlan-Apochromate 1.4 NA objective and standard *epi*-fluorescence filters. Data are given as averages of at least 15 animals per genotype from three independent experiments.

2.4. Gene expression analyses

Transcriptional activation of *C. elegans* ced-13 and *egl-1* was measured in synchronized N2 and nth-1 L4 hermaphrodites after treatment with paraquat, as described above. For total RNA extraction, worms were disrupted in TRIZOL with 0.7 mm zirconia/silica beads (Biospec Products) using a Mini-Beadbeater 8 (Biospec Products) at maximum speed for 30 s. cDNA synthesis was performed using iScript cDNA synthesis kit (Bio-Rad), according to the manufacturer's instructions. Quantitative reverse transcriptase PCR (qRT-PCR) was performed with SYBR Green supermix (Bio-Rad). *ced-13* and *egl-1* transcript levels were normalized to an internal tubulin (*tbg-1*) control. *sod-3* transcript levels were normalized to Y45F10D.4 control. Primers (Eurogentech) with the following sequences were used: for *egl-1* (5-CCTCAACCTCTTCGGATCTT-3) and (5-TGCTGATCTCAGAGTCATCAA-3); for *ced-13* (5-GCTCCCTGTTTATCACTTCTC-3) and (5-CTGGCATACGTCTTGAATCC-3); for *tbg-1* (5-AAGATCTATTGTTCTACCAGGC-3) and (5-CTTGAACTTCTTGTCCTTGAC-3); for *sod-3* (5-gtcgcttcaaatcagttcagc-3) and (5-gttcttgtcaagtgatccgaca-3); for Y45F10D.4 (5- CTAAGGATGGTGGAGAACCTTCA-3) and (5-CGCGCTTAATAGTGTCCATCAG-3).

As a control of RNAi efficiency, mRNA expression levels were measured after three generations of feeding N2 animals on *E. coli* expressing RNAi, targeting the indicated genes. The primers were as follows (sense strand): *xpa-1* forward: (5-CTTGGTGGCGGATTCTGTGA-3), reverse: (5- TCCCAAAGCCAACTGTCCAT-3); *xpc-1* forward: (5-TTTCCCCATCCAAACGTGCT-3); reverse: (5- AGGGCTTGATATTGGTCGTCG-3); *csb-1* forward: (5-GATGCCAAGAGAGCCAGGAA −3); reverse: (5-GAATAATGGGAGCAAATGCGGT-3).

2.5. Immunohistochemistry

Animals were collected 24 h after treating synchronized L4 hermaphrodites with 400 μM paraquat. Germlines were dissected on poly-L-lysine-coated slides in egg buffer (25 mM HEPES, pH 7.4, 118 mM NaCl, 48 mM KCl, 2 mM $CaCl_2$, 2 mM $MgCl_2$) supplemented with 0.1% Tween-20 and 0.2 mM levamisol. Germlines were fixed in 4% formaldehyde for 5 min at room temperature and freeze-cracked in liquid nitrogen. Next, the germlines were fixed in 1:1 acetone:methanol for 10 min at −20 °C, washed in PBS-T (1 x PBS, 0.1% Tween-20) for 5 min, followed by 30 min incubation with image-IT FX signal enhancer (Invitrogen) and 30 min blocking in PBS-TB (1 x PBS, 0.1% Tween-20, 0.5% BSA). The slides were incubated with primary antibody overnight at 4 °C, washed three times for 10 min in PBS-T, followed by incubation with the secondary antibody at room temperature for 2 h. Finally, the germlines were washed three times for 10 min in PBS-T and mounted with 7 μl mounting solution containing ProLong Gold (Thermo Fisher) and 0.5 μg/ml DAPI (Sigma). Primary antibodies were used at the following dilutions: pPMK-1 (1:200), pJNK-1 (1:200), pH3 (1:400), and RAD-51 (1:20 000) (a gift from Sarit Smolikove). The secondary antibody used to detect was Alexa 488- conjugated anti-rabbit at 1:1500 dilution and cy3 at 1:1000 dilution.

2.6. Quantification of ATP and reactive oxygen species (ROS) content in C. elegans whole-cell extracts

For ATP and ROS measurements, populations of ~1000synchronized young adult animals were collected in S-Basal, washed twice, immediately frozen in liquid nitrogen and stored at −80° C. Frozen worms were then thawed on ice and subjected to sonication (see western blot procedure) in a final volume of 300 µl of S-Basal containing protease-inhibitor cocktail (Sigma-Aldrich). ATP levels were immediately measured in 25 µg of extract using the ATP Bioluminescence Assay Kit CLS II (Roche) according to the manufacturer's protocol. Each biological sample was divided into two duplicate wells in flat bottom 96-well dark plates and measured in an Infinite® 200 PRO (Tecan) microplate reader. Each assay included a negative control with no extract. ROS levels were quantified utilizing 50 µg of extract incubated in 500 µl of a 5 µM H2-DCF-DA (2′-7′-dichlorofluorescein-diacetate) solution in S-Basal containing protease-inhibitor cocktail. Each sample was read in triplicate (150 µl each) in a flat bottom 96-well plate in an Infinite® 200 PRO (Tecan) microplate reader at excitation/emission wavelengths of 485 and 528 nm. Different readings were carried out over a time frame of 2 h to ensure that the reaction was occurring properly (the initial fluorescence was always subtracted from the last reading). Data collected at the one-hour time-point are shown as the average ± SD. Student *t*-tests were performed to assess statistical significance.

2.7. Measurement of steady-state ROS levels and mitochondrial membrane potential by confocal microscopy

In vivo relative steady-state ROS levels and mitochondrial membrane potential (ΔΨM) was determined using fluorescent confocal microscopy. Two independent, age-synchronous populations were generated using a standard treatment with 20% alkaline hypochlorite; half of each population was reserved to create line-specific internal control groups. Confocal image analysis was performed on live young adult nematodes using our previously described method [17–19]. Briefly, nematodes were incubated for 24 h at 20 °C in the presence or absence of 10 µM MitoSOX or 10 µM Mitotracker Red CMXRos (Molecular Probes Inc.) for ROS and ΔΨM assays, respectively. Fluorescent z-stack images of the pharyngeal bulbs of 17–20 worms from each treatment and 5 control nematodes that had been immobilized by levamisole were captured at 60X magnification using an Olympus IX71 inverted microscope mounted with a Nikon Coolsnap ES2 HQ camera and a short arc 250W Xenon lamp, all part of a high resolution wide field Core DV system (Applied Precision™; Oregon Health and Sciences University Advanced Light Microscopy Core Facility, Portland, OR). Deconvolution-optimized images were used to quantify relative ROS and ΔΨM levels by manually enclosing the terminal pharyngeal bulb within each image and obtaining the average intensity of the area using ImageJ software. Since maximum fluorescence measures offer greater consistency as they do not depend upon pixel size or on the number/area of fluorescent signals within an image we analyzed maximum values of fluorescence as before [18]. Final ROS and ΔΨM levels were calculated as the difference between pharyngeal bulb intensity in labeled and unlabeled control worms from each strain.

2.8. Western blot analysis

Quantification of GST-4:GFP protein levels in the transgenic CL2166 strain was performed on whole-worm protein extracts prepared from ~200 adult worms. Upon collection in S-Basal, animals were washed and then immediately frozen in liquid nitrogen. Samples were subsequently thawed on ice, subjected to two cycles of sonication for ten seconds (30% power, 30% amplitude) in a BANDELIN SONOPLUS HD 3100 sonicator in a final volume of 300 µl of RIPA buffer containing protease-inhibitor cocktail (Sigma-Aldrich), and centrifuged at 4° C for 15 min to eliminate insoluble debris. Following total protein quantitation of the supernatant by the Bradford assay, GST-4 protein levels were measured by western blot analysis, quantified using ImageJ software, and normalized against actin. SDS-polyacrylamide gel electrophoresis and western blotting were performed according to standard protocols. Briefly, total worm extract was separated on 12.5% or 4–20% Criterion gels (Bio-Rad). Nitrocellulose membranes were blocked in TBS containing 0.5% Tween 20, and 5% non-fat dry milk or BSA for 1 h at room temperature and incubated with the following primary antibodies: pPMK-1 (1:200), anti-GFP (Clontech, 1:1000), and anti-Actin (clone AC-15, Sigma-Aldrich, 1:5000) at 4 °C overnight. Anti-rabbit (Cell Signaling, 1:10 000) secondary antibody was incubated at room temperature for 1 h.

2.9. Mitochondrial DNA copy number quantification

Determination of mitochondrial DNA (mtDNA) copy number was quantified using Real Time-quantitative PCR (qPCR). Genomic DNA from L4 larvae and young adult worms was isolated using a DNA extraction kit (DNeasy Blood and Tissue Kit, Qiagen). qPCR was performed using SYBR GREEN PCR Master Mix (Applied Biosystems) using the following primers (Eurogentech): the *act-3* forward primer (5-TGC GACATTGATATCCGTAAGG-3) and reverse primer (5-GGTGGTTCCTC CGGAAAGAA-3). *nd-1* forward primer (5-AGCGTCATTTATTGGGAAG AAGAC-3) and reverse primer (5-AAGCTTGTGCTAATCCCATAAATGT-3). *nd-5* forward primer (5- TTAGCAAGTTTGGTCGAAGAAGATT-3) and reverse primer (5- GGCCCAAAGTAACTATTGAAAAACC-3). Data were calculated using the absolute quantification method from a standard-curve for each primer set and the mtDNA copy number was calculated as the amplification of the mitochondrial gene relative to the amplification of the nuclear gene. The experiments were repeated at least 3 times and are presented as relative to L4 N2.

2.10. Respiration analyses

Oxygen consumption of nematodes at 20 °C was determined using an Oxygraph–2 K (Oroboros, Innsbruck, Austria). The integrated software (DATLAB 4.2) presents respiration as oxygen flux; pmol O_2/nematode. 400 freshly picked animals were placed on non-seeded NGM plates followed by immediate transfer to the oxygraph filled with M9 buffer stirred at 300 rpm. To obtain reproducible results, we performed the experiments within identical times from harvest. We report two values: the initial respiration after closure of stoppers in the oxygraph (Vo), and the stable level of respiration (V1), measured 5 min after closure. The difference (V0-V1) is ascribed to sensitivity to oxygraphy measurement (e.g. stirring).

3. Results

3.1. C. elegans NTH-1 is an active DNA glycosylase

We confirm previous studies [7] showing that purified NTH-1 has activity on thymine glycol-containing oligonucleotides (Supplementary Fig. S1A and B). Still, we observed no reduction in the capacity to repair the classical NTH-1 substrates 5-hydroxycytosine or 5-hydroxyuracil in whole-worm extracts prepared from *nth-1*(*ok724*) mutants (Supplementary Fig. S1C). In the absence of exogenous stressors, *nth-1* mutants have normal embryonic viability and self-brood size (Supplementary Table S1). Spontaneous and heat-shock induced male frequencies, increases of which are associated with genomic instability in *C. elegans*, were indistinguishable from the isogenic wild-type strain (Supplementary Table S1). Finally, the spontaneous mutant frequency measured in the classical *unc-58* reversion assay was not elevated in the *nth-1;unc-58* mutant compared to the *unc-58* strain (Supplementary Table S2). Hence, although NTH-1 has DNA glycosylase activity *in vitro*, *nth-1* mutants do not show any obvious genomic instability phenotype.

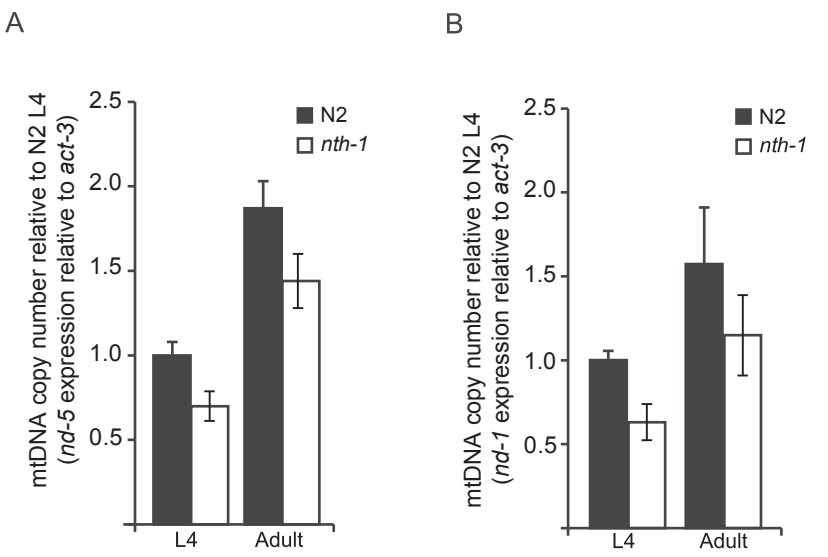

Fig. 1. Reduced mtDNA copy number in *nth-1*. Mitochondrial DNA (mtDNA) copy number was measured using quantitative PCR amplification of the mitochondrial genes (A) *nd-5* and (B) *nd-1* relative to a single copy nuclear gene *act-3* in L4 larvae and young adult worms in the wild type N2 strain (black bars) and the *nth-1* mutant (white bars). mtDNA copy number relative to N2 L4 is shown. The data represent the average ± SD from three independent experiments. Statistical significance between mtDNA copy number in N2 versus *nth-1* were evaluated by a two-tailed Student *t*-test. For *nd-5* ($p = 0.002$) and ($p = 0.0002$) and for *nd-1* ($p = 0.00003$) and ($p = 0.1$) at L4 and adult stages, respectively.

3.2. Reduced mitochondrial copy number in nth-1

Like its human counterpart [20,21], *C. elegans* NTH-1 is predicted to have both nuclear and mitochondrial localization [7]. No defect in mitochondrial DNA repair was previously observed in the *nth-1*(*ok724*) mutant using a qPCR-based assay, but the authors observed that the mitochondrial DNA copy number was less stable in the *nth-1* mutant following exposure to H_2O_2 [14]. To further elucidate whether *C. elegans* NTH-1 may contribute to maintain mitochondrial integrity, we measured the mitochondrial genome (mtDNA) copy number. The *nth-1* mutant showed the expected developmental increase in mtDNA copy number from the L4 stage to adulthood [22]. However, the mtDNA copy number was significantly lower in *nth-1* mutants compared to the isogenic wild-type strain when measured as the amplification of two different mitochondrial genes, *nd-1* and *nd-5*, relative to the single-copy nuclear gene *act-3* (Fig. 1). The *nth-1* mutant had lower mtDNA copy number compared to the N2 control at both developmental stages, with 50% reduction in L4 larvae ($p < 0.05$) and a 19% reduction in young adults ($p < 0.05$) when measured as the amplification of *nd-5* relative to *act-3* (Fig. 1A). Reduced mtDNA copy number was also observed at the L4 stage when measured with respect to *nd-1*, which showed reductions of 37% ($p < 0.005$) at the L4 stage. The 27% reduction in the mtDNA copy number with respect to *nd-1* in adult *nth-1* was not statistically significant (Fig. 1B).

3.3. Increased steady-state ATP and ROS levels in nth-1

Next, we tested whether the reduction in mtDNA copy number was accompanied by changes in mitochondrial function. Mitochondria are the main cellular source of ATP in well-fed animals. To test whether the reduction of mtDNA copy number led to changes in steady-state ATP levels, we used a standard ATP Bioluminescence Assay. Surprisingly, *nth-1* whole- worm extracts had 3.4-fold higher steady-state ATP levels compared to the isogenic wild-type strain (Fig. 2A). If the increased ATP levels resulted from increased mitochondrial ATP production, this phenotype should be accompanied by increased oxygen consumption. We therefore measured O_2-consumption using an Oxygraph–2 K. However, both the initial respiration (Vo) and the stable level of respiration (V1) were unchanged in *nth-1* mutants (Fig. 2B and C, respectively). Thus, reduced mtDNA copy numbers are not accompanied by reduced mitochondrial respiration or ATP deficit in the *nth-1* mutants. Normal pharyngeal pumping rates in the *nth-1* mutant supports that neuromuscular functionality is maintained in the *nth-1* mutant despite reduced mtDNA copy number (Supplementary Fig. S2). Such disconnect between ATP levels and oxygen consumption may indicate that there might be reduced ATP consumption in the *nth-1* mutant or, alternatively, that ATP levels are maintained through alternative biosynthetic pathways.

Previous gene expression profiling showed that several genes responding to oxidative stress were upregulated in *nth-1* mutants [13], including genes transcriptionally activated by SKN-1, the *C. elegans* ortholog of human Nrf2 [23]. Quantitative RT-PCR confirms that the expression of the SKN-1-responsive gene *sod-3*, a mitochondrial Fe/Mn-dependent superoxide dismutase, was increased in the *nth-1* mutant relative to a constitutively expressed housekeeping gene Y45F10D.4 (Fig. 2D). To show that GST-4 was upregulated also on the protein level, we crossed the *nth-1* mutant into a transgenic strain expressing GST-4 as a translational fusion with GFP led to a 54% increase ($p < 0.001$) in the expression of the GST-4:GFP protein in the *nth-1* mutant compared to the wild type control (Fig. 2E). Thus, there is an upregulation of SKN-1 responsive genes in the *nth-1*(*ok724*) strain.

As SKN-1 is the main sensor of oxidative stress in *C. elegans*, we suspected that SKN-1 activation reflected chronic oxidative stress in the *nth-1* mutant. To verify this we took advantage of a ROS-sensitive probe H2-DCF-DA and found a 29% increase ($p < 0.001$) in the steady-state ROS level in extracts prepared from *nth-1* (Fig. 2F). Measurement of *in vivo* ROS levels using microscopy showed a 3.7-fold increase ($p < 0.001$) in the *nth-1* mutant (Fig. 2G). The increased ROS may stem from increased leakage from the mitochondrial electron transport chain as the mitochondrial membrane potential was reduced 2.4-fold ($p < 0.001$) in the *nth-1* mutant compared to the N2 strain (Fig. 2H).

Taken together, these results show that *C. elegans nth-1* experiences chronic oxidative stress and mitochondrial dysfunction, characterized by reduction in mtDNA content and mitochondrial membrane potential and higher *in vivo* ROS levels.

3.4. C. elegans nth-1 is unable to induce apoptosis in response to paraquat

Mitochondria are important regulators of apoptosis in several species including *C. elegans* (reviewed in [24]). Thus, we asked whether the DNA repair defect, combined with mitochondrial dysfunction, in the *nth-1* mutants affected their ability to mount an apoptotic response to the superoxide generator paraquat, which is known to induce apoptosis in the *C. elegans* germline [25], but also generates oxidised DNA bases. To monitor apoptosis *in vivo*, we crossed the *nth-1* mutant with a transgenic reporter strain expressing the apoptotic cell engulfment receptor CED-1 in fusion with GFP [3].

Contrary to what might be expected from a DNA repair mutant, the

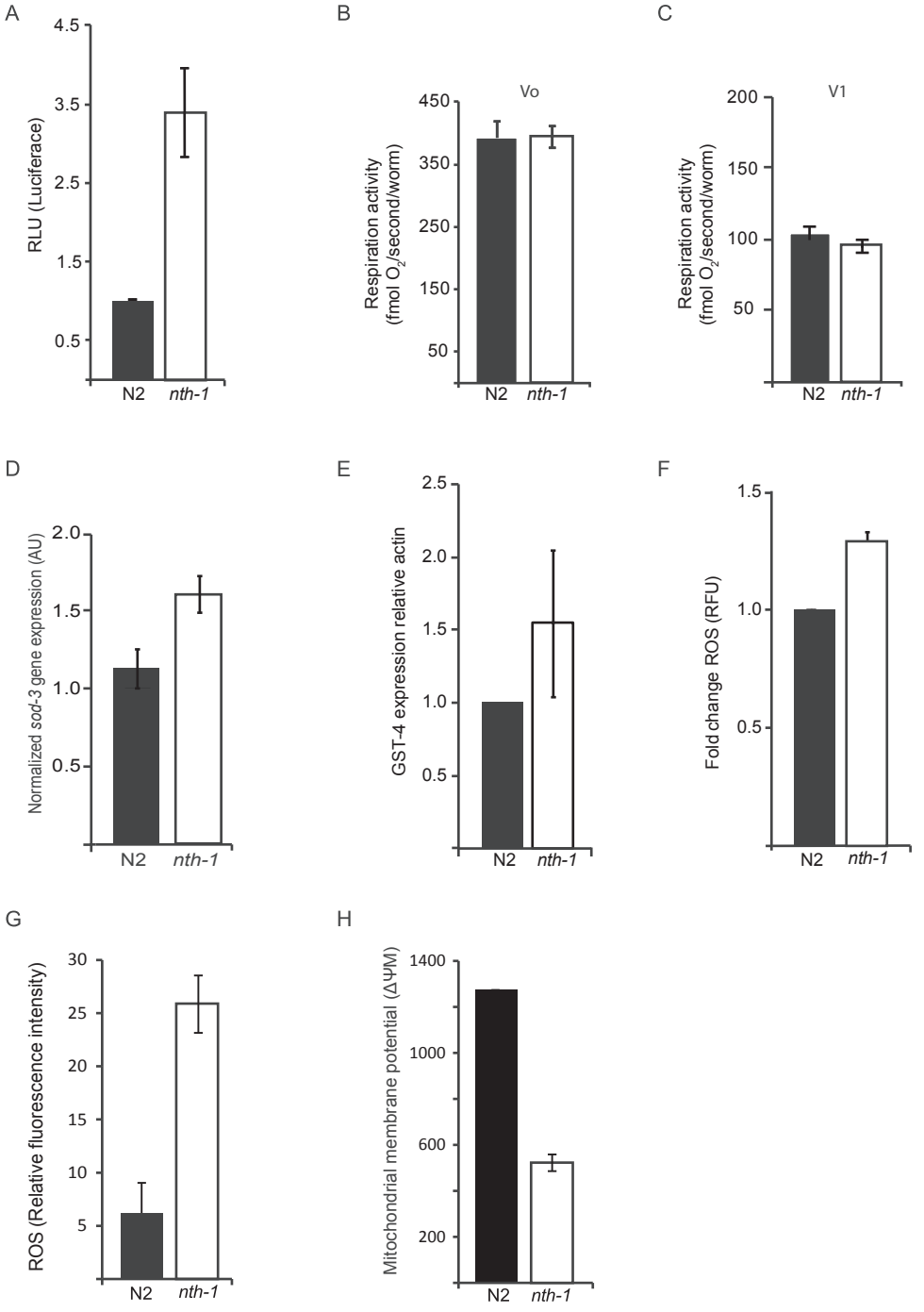

Fig. 2. Increased steady state ATP and ROS levels in *nth-1*. (A) ATP levels were measured using a standard ATP Bioluminescence Assay Kit. (B and C) O_2-consumption was measured using Oxygraph–2 K in young adult worms. The initial respiration after closure of stoppers in oxygraph (Vo), and the stable level of respiration, measured 5 min after closure (V1). (D) Expression of *sod-3* mRNA relative to a house-keeping gene Y45F10D.4 was measured by qRT-PCR. (E) GST-4 expression was evaluated from western blot analysis using anti-GFP antibodies. Expression of GST-4:GFP was measured relative to an actin loading control. (F) The ROS sensitive probe H2-DCF-DA was used to measure ROS levels in whole worm extracts. (G) *in vivo* ROS measured as relative fluorescence intensity measured in the presence of MitoSOX. (H) Mitochondrial membrane potential ΔΨM measured in the presence of Mitotracker Red CMXRos. All data represent the mean ± SD of three independent experiments from N2 (black bars) and *nth*-1 (white bars). Statistical significance was evaluated by a two-tailed Student *t*-test. (For interpretation of the references to colour in this figure legend, the reader is referred to the web version of this article.)

nth-1-deficient animals showed a severely attenuated apoptotic response to paraquat. Whereas 13 CED-1:GFP positive apoptotic corpses (4.3-fold induction) were detected in wild type animals 24 h after exposure to 400 µM paraquat, on average, only 6 corpses (1.5-fold) were detected in *nth-1* mutants (Fig. 3A). There was no induction of the *C. elegans* p53 ortholog CEP-1-target genes *ced-13* and *egl-1* in paraquat-treated NTH-1 deficient animals (Fig. 3B), consistent with previous findings that paraquat-induced apoptosis is independent of CEP-1 [25]. The core apoptotic machinery is functional in *nth-1* mutants as demonstrated by a robust induction of apoptosis in response to the alkylating agent ethylnitrosourea (ENU) (Fig. 3A and B), which induces apoptosis in a CEP-1 dependent manner [26]. The reduction in apoptotic-corpse formation could not be explained by a reduction of apoptosis-competent pachytene-staged cells (Fig. 3C). However, when cultivated under standard growth conditions, the *nth-1* mutant had a significantly reduced number of cells in the mitotic region (Fig. 3D), which was also reflected by a lower number of cells staining positively for the G2/M-phase marker phospho-ser10 Histone 3 (PH3) (Fig. 3E). The mitotic index, calculated as the fraction of PH3-positive cells in the mitotic zone was identical in the *nth-1* mutant and the wild type (0.12 PH3-positive cells/total number of cells), indicating that there was no defect or block in cell-cycle progression in the mutant. In paraquat-treated animals, the number of mitotic cells was indistinguishable in *nth-1* and the wild type (Fig. 3D). This effect was caused by a reduction of mitotic cells in the wild type strain, while the number of germline mitotic cells in *nth-1* mutants was unaffected by paraquat treatment. Thus, *nth-1* mutants fail to induce cell-cycle arrest and robust apoptotic response following treatment with the superoxide generator paraquat.

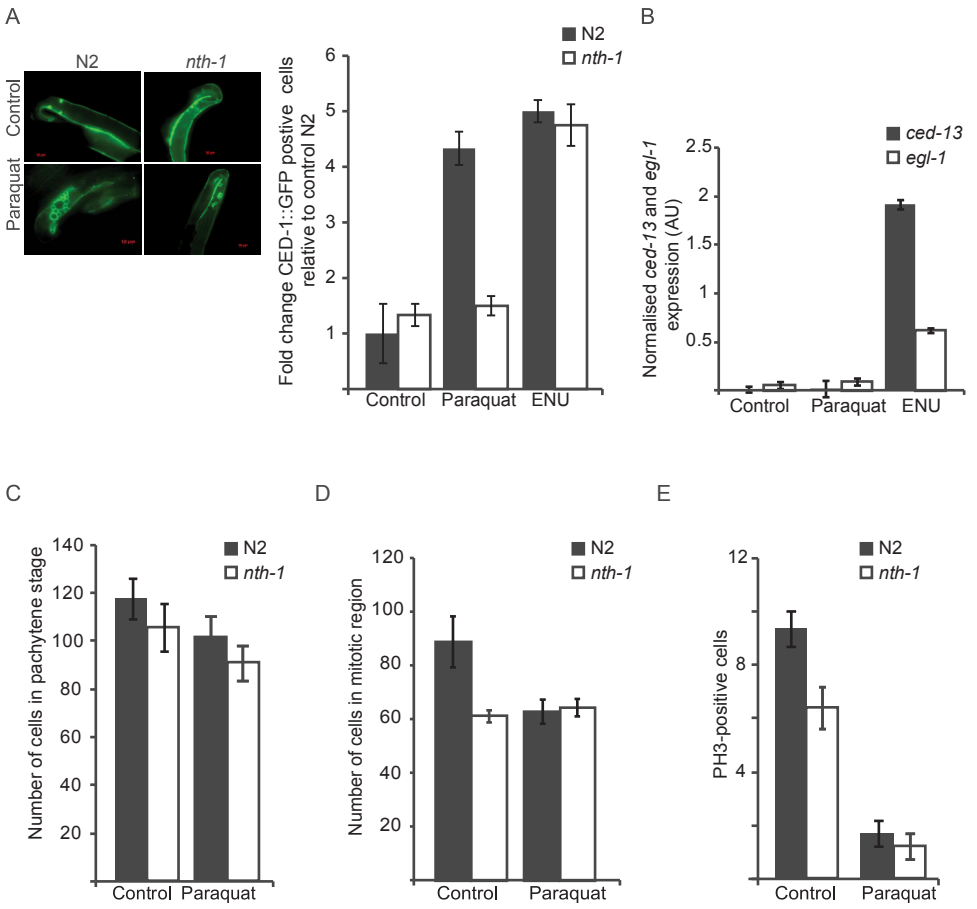

Fig. 3. Loss of NTH-1 attenuates paraquat-induced apoptosis. (A) Apoptotic cell corpses (left panel) were quantified in the transgenic NTH-1 proficient *ced-1:gfp* strain (black bars) and *nth-1;ced-1:gfp* (white bars) 24 h after treatment with 400 μM paraquat and 5 mM ENU. The number of apoptotic cell corpses per gonad arm was counted in more than 20 germlines per experiment and is given as the relative induction ± SEM compared to the basal level for each strain from three to four independent experiments. (B) Expression levels of the CEP-1 target genes *egl-1* (white bars) and *ced-13* (black bars) relative to *tbg-1* were measured by qRT-PCR from RNA extracted from young adult *nth-1* mutants 24 h h after exposure to paraquat or ENU. Data is given as average ± SEM from three independent experiments. (C) For analysis of meiotic germ cell number, DAPI stained germline nuclei were quantified in the meiotic region from at least 15 germlines and given as average ± SD. (D) The number of cells in the mitotic region was quantified by counting DAPI-stained mitotic germ cells from images captured in one single optical section in at least 15 germlines and given as average ± SD. (E) For quantification of the number of G2/M-phase cells, dissected germlines were subjected to immunohistochemistry and stained with antibodies recognizing phospho-ser10 Histone 3 (PH3). The number of PH3-positive cells was quantified in the mitotic zone. Data are given as average ± SD from at least 15 germlines. Panels B, C, and D shows results from N2 (black bars) and *nth-1* (white bars).

3.5. Constitutive PMK-1 and JNK-1 activation in C. elegans nth-1 mutants

Paraquat induces apoptosis in a CEP-1 independent manner through pathways that depend on the redundant activities of several conserved stress-responsive mitogen-activated protein kinase (MAPK) pathways [25]. As both the reduction of germline mitotic cell numbers and the attenuated apoptotic response would be consistent with a disturbance in pathways involving these kinases, we tested whether paraquat was able to activate the MAPK PMK-1, which is required for pathogenesis-[27] and arsenite- induced germ cell apoptosis [28]. To test whether PMK-1 was activated in the germline in response to paraquat, we followed phosphorylation of PMK-1 (pPMK-1) by immunohistochemistry (Supplementary Fig. S3A) and measured the average intensity of pPMK-1 staining in the mitotic and meiotic compartments separately. Phosphorylation of PMK-1 was observed in both the mitotic and meiotic germline compartments in response to paraquat, but whereas the wild type had a 1.9 −fold increase of pPMK-1 signal intensity ($p = 0.0001$) in the pachytene zone, the *nth-1* mutant had a lower, 1.2-fold induction ($p = 0.001$) (Fig. 4A). There was no difference in the pPMK-1 signal intensity between *nth-1* mutant and the wild type after paraquat treatment, but the *nth-1* mutant had significantly higher intensity of pPMK-1 staining throughout the germline in the untreated condition (1.3- and 1.5-fold higher in the mitotic and pachytene regions, respectively). Similar results were obtained by western blotting of pPMK-1 in total cell extracts prepared from young adults, suggesting that basal pPMK-1 levels were also high in somatic tissue (Supplementary Fig. S4A). Thus, paraquat induces pPMK-1 in both strains, but *nth-1* mutants have higher basal PMK-1 phosphorylation.

JNK-1 is known to regulate DNA-damage induced apoptosis in *Drosophila melanogaster* and in mammalian cells [29,30], but whether it does so in *C. elegans* is not clear. However, JNK-1 are among several stress-activated MAPK redundantly required for CEP-1 independent apoptosis in response to arsenite, an inducer of oxidative stress [28]. To test whether JNK-1 was also activated in response to paraquat, we followed phosphorylation of JNK-1 (pJNK-1) in the germline (Supplementary Fig. S3B). Weak staining for pJNK-1 was seen in both the mitotic and pachytene regions of the germline in the wild type strain under basal conditions (Fig. 4B). As observed for PMK-1, the *nth-1* mutant had higher basal pJNK-1 staining in both germline compartments (Fig. 4B). Compared to the wild type counterpart, the *nth-1* mutant had 2.7-fold ($p = 0.0001$) and 4-fold ($p = 0.0001$) higher basal pJNK-1 staining intensity in the mitotic and pachytene zones, respectively.

After paraquat exposure, pJNK-1 was induced in the wild type strain with staining intensity increasing across the germline, with 3.9-fold induction ($p = 0.0001$) in the mitotic region and 6-fold induction ($p = 0.0001$) in the pachytene region. In paraquat treated *nth-1* mutants, the additional increase in signal intensity was modest with 1.3-fold ($p = 0.009$) and 1.1-fold ($p = 0.0006$) induction in the mitotic region and pachytene zone, respectively (Fig. 4B).

Taken together, *nth-1* mutants experience by chronic oxidative stress and higher basal activation of the stress responsive kinases, PMK-1 and JNK-1, concomitant with attenuated response to paraquat.

3.6. Loss of GG-NER restores apoptosis induction and reduced JNK-1 activation in nth-1 mutants

As CEP-1 dependent apoptosis is functioning normally in *nth-1* mutants (Fig. 3A), we asked whether the chronic oxidative stress, including high basal MAPK activation, could be an underlying cause of the failure of *nth-1* mutants to induce apoptosis in response to paraquat. If so, we would expect that the ability to induce apoptosis would be regained if the compensatory cellular stress responses were attenuated. It has been shown that PMK-1 is required for induction of apoptosis in

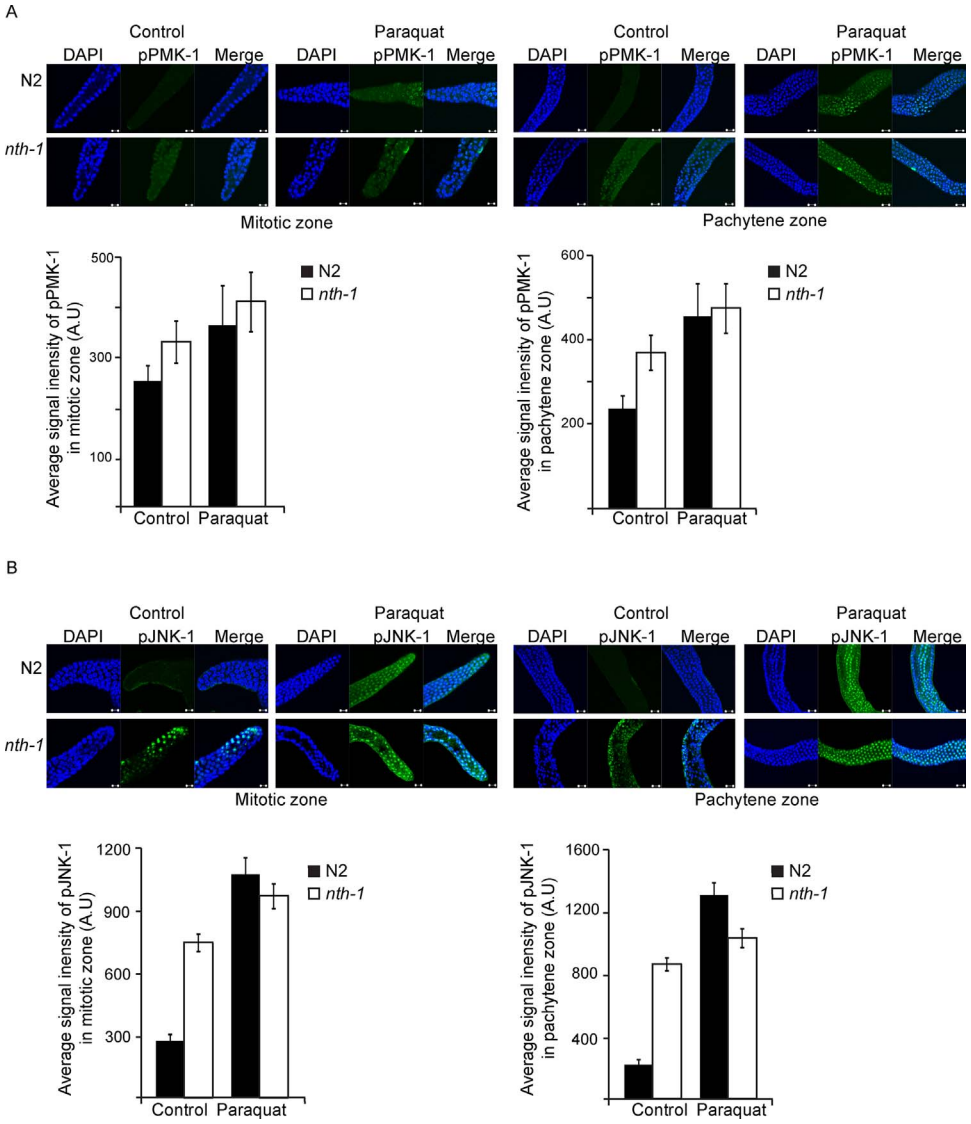

Fig. 4. Attenuated MAPK activation in response to paraquat in nth-1. (A) pPMK-1 staining in the mitotic (left panel) and pachytene (right panel) regions of young adult *nth-1* and wild type germlines, either untreated (control) or 24 h after 400 µM paraquat treatment. Nuclei were stained with DAPI. Average signal intensity of pPMK-1 staining was quantified in a 40×10^7 nm^2 area in the mitotic zone (left panel) and 120×10^7 nm^2 area in the pachytene zone (right panel). (B) pJNK-1 staining in the mitotic (left panel) and pachytene (right panel) regions of young adult *nth-1* and wild type germlines, either untreated (control) or 24 h after paraquat treatment. Average signal intensity of pJNK-1 staining was quantified as above. The graphs represent mean ± SD from at least 15–20 germlines for each condition. Two-tailed Students *t*-tests were used to evaluate significance.

response to paraquat [25]. Here, we confirm this observation in wild type animals (Supplementary Fig. 4E) and it was therefore not surprising that depletion of PMK-1 by RNAi was unable to restore apoptosis in the *nth-1* mutant (Supplementary Fig. 4E). Similarly, depletion of JNK-1 by RNAi suppressed germline apoptosis in the both wild type and in *nth-1* mutants (Supplementary Fig. S4E), suggesting that JNK-1 contributes to paraquat-induced apoptosis as it does for arsenite [28]. Therefore, depletion of PMK-1 or JNK-1 could not restore apoptotic response to paraquat.

However, we showed previously that activation of the compensatory stress response depended on a collaboration between NTH-1 and DNA damage recognition proteins of the Nucleotide Excision Repair (NER) pathway [13,31]: We showed that there was no induction of SKN-1 or other oxidative stress response genes in *nth-1* mutants (Fig. 2D, 2E) that also lacked the NER protein XPA-1 [13]. Thus, we tested whether the high basal activation of JNK-1 in the germline, which is part of this compensatory program, was suppressed by depleting key NER proteins. In support of this hypothesis, depletion of XPA-1 resulted in markedly suppressed basal pJNK-1 staining in *nth-1* germlines while there was no effect on basal pJNK-1 staining in untreated wild type controls (Fig. 5A). As expected from our previous studies [31], this effect was not exclusive to XPA-1, but was seen also after depletion of XPC-1, which is required for DNA damage detection in global genome NER (GGR). Depletion of CSB-1, which is required for transcription-coupled repair in somatic cells, but not required for UV-induced apoptosis in the germline [32], also suppressed basal JNK-1 phosphorylation in the *nth-1* mutant but not to the same extent as XPA-1 and XPC-1 depletion (Fig. 5A). Depletion of XPA-1 and XPC-1 did not prevent JNK-1 phosphorylation in response to paraquat in wild type animals (Fig. 5B), but no JNK-1 phosphorylation was seen in the *nth-1* mutants (Fig. 5B). Depletion of CSB-1 suppressed JNK-1 phosphorylation following paraquat treatment in wild-type animals and, to a lesser extent, also in *nth-1* mutants (Fig. 5A and 5B). Thus, the basal activation of JNK-1 in the *nth-1* mutant is a consequence of the compensatory stress response elicited through genetic interactions between DNA damage recognition proteins of the BER and GG-NER pathways.

If the attenuated apoptotic response following paraquat treatment of the *nth-1* mutant resulted from high basal JNK-1 phosphorylation, we would expect that the apoptotic response would also be regained by depleting XPA-1 and XPC-1, but perhaps not in CSB-1 depleted animals as JNK-1 seemed to be required for robust apoptotic response to paraquat (Supplementary Fig. S4E) and *csb-1* RNAi interfered with JNK-1 phosphorylation (Fig. 5B). In support of this hypothesis, the number of apoptotic corpses induced by paraquat in *nth-1* depleted for XPA-1 or XPC-1 by RNAi was indistinguishable from the wild type (Fig. 5C). The basal level of apoptotic corpses was unchanged in wild type and *nth-1* mutants under these conditions, showing that apoptosis induction depended on paraquat treatment (Supplementary Fig. S4C). Suppression

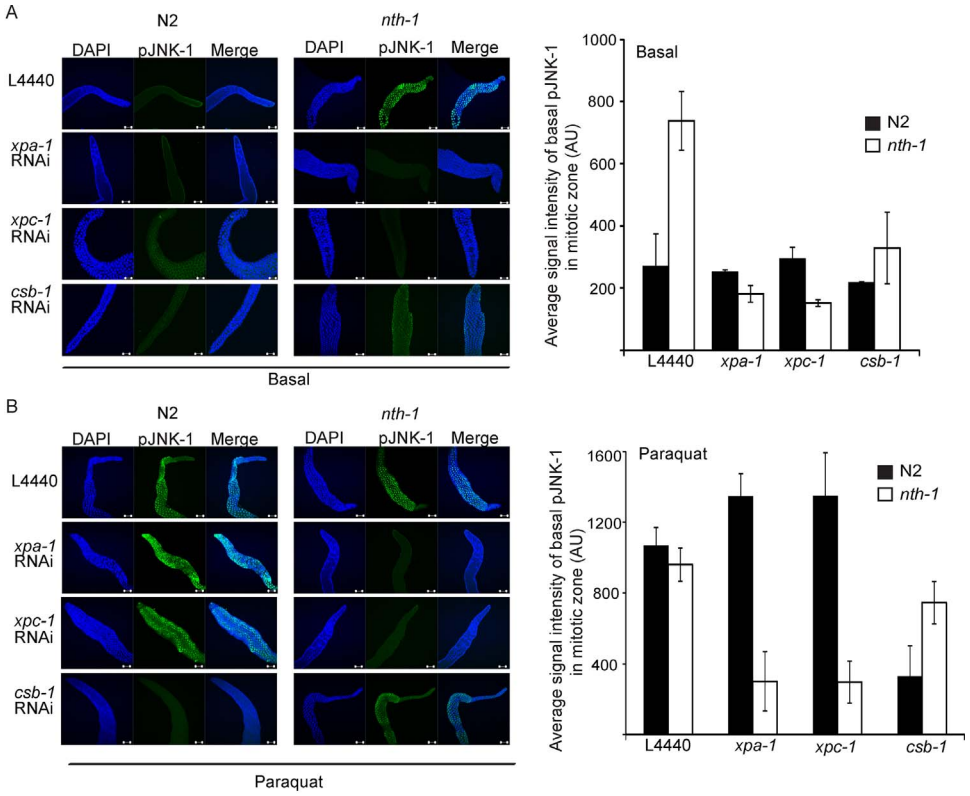

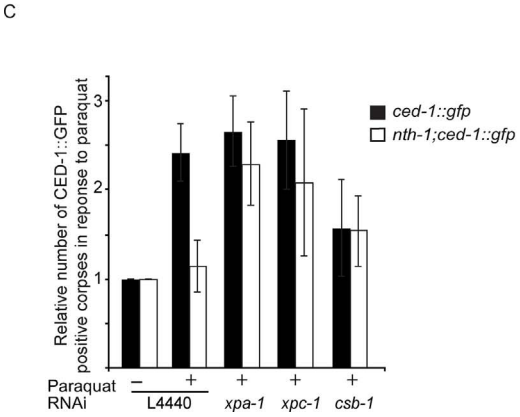

Fig. 5. Suppression of basal JNK-1 phosphorylation restores paraquat-induced apoptosis in nth-1. N2 wild type (left panels) and *nth-1* mutants (right panels) germlines were extracted 24 h after the L4 stage from untreated animals (A) or after treatment with 400 μM paraquat from the L4 stage (B). The germlines were stained with pJNK-1 antibodies. Nuclei were stained with DAPI. Average signal intensity of pJNK-1 staining was quantified in a 40×10^7 nm^2 area in the mitotic zone. The graphs represent mean value ± SD from at least 15–20 germlines for each condition. Two-tailed Students *t*-tests were used to evaluate significance. (C) The transgenic NTH-1 proficient *ced-1:gfp* strain WT (black bars) and *nth-1;ced-1:gfp* (white bars) were cultured on empty vector control RNAi (L4440) or RNAi targeting the indicated genes. Apoptotic cell corpses were quantified in 24 h after treatment with 400 μM paraquat. The average number of apoptotic cell corpses per gonad arm was determined from more than 20 germlines per experiment and is given as the relative induction ± SEM compared to the basal level for each strain from three to four independent experiments.

of transcription-coupled repair by depleting CSB-1 gave less efficient suppression of basal pJKN-1 staining (Fig. 5C) even though the RNAi efficiency was comparable to that of *xpa-1* and *xpc-1* RNAi (Supplementary Fig. S4D). Depletion of CSB-1 did not result in a statistically significant increase of paraquat-induced apoptotic corpses compared to *nth-1* mutants fed control RNAi (Fig. 5C). Thus, the inability to mount an apoptotic response to paraquat in the *nth-1* mutant correlates with high basal JNK-1 phosphorylation but not the paraquat induced JNK-1 phosphorylation level.

Taken together, our data support the conclusion that failure to induce apoptosis in *nth-1* mutants is not a direct consequence of the DNA repair defect. Instead, attenuation of the apoptotic responses to paraquat in *nth-1* is a side effect of the activation of compensatory stress response pathways, which include increased basal JNK-1 phosphorylation in the germline.

4. Discussion

4.1. Repair of oxidative DNA damage in C. elegans

NTH-1 is the only *C. elegans* DNA glycosylase known to initiate repair of oxidised bases through the BER pathway. NTH-1 has activity on classical NTH substrates like 5-hydroxycytosine and thymine glycol (this study and [7]), but we observed no BER defect nor increased mutation frequency in the *nth-1;unc*-58 mutant compared to the *unc-58* reference strain. In contrast, *C. elegans ung-1* mutants show elevated spontaneous mutation frequency when measured in both the *unc*-58 reversion assay [5] and in a transgenic mutation-reporter assay [33]. Thus, it may be that other DNA repair pathways, such as NER, are more important than BER to repair oxidative DNA damage [34]. It is also possible that the upregulation of oxidative stress responses [13] counteracts damage accumulation [31].

4.2. Bioenergetic changes in C. elegans nth-1

In contrast to the lack of a clear DNA repair defect, *C. elegans nth-1*

mutants have a mild mitochondrial dysfunction phenotype with reduced mitochondrial DNA content and reduced mitochondrial membrane potential. This was accompanied by increased steady-state ROS levels, an expected consequence of mitochondrial dysfunction but, surprisingly, also by increased ATP levels. This apparent discrepancy would suggest that the mitochondrial dysfunction in *nth-1* mutants causes a bioenergetic shift away from oxidative phosphorylation (explaining the high ROS and low mitochondrial membrane potential) to alternative pathways such as aerobic glycolysis, which would be consistent with high ATP levels [35]. High ATP levels would also be consistent with increased reliance on mitochondrial- or peroxisomal-beta oxidation which is supported by the *nth-1* transcriptome [13].

Mitochondrial dysfunction and altered bioenergetic profiles are emerging as a prominent phenotype in several DNA repair mutants. We have previously shown that mitochondrial dysfunction is seen in *xpa-1* [36], *csb-1* [37], and *atm-1* mutants [38]. In these mutants the mitochondrial dysfunction is, at least partly, an indirect consequence of constitutive PARP1 over-activation, which leads to depletion of cellular NAD^+ pools, defects in mitochondrial biogenesis, and clearance of dysfunctional mitochondria. We have not been able to detect PARP-1 over-activation in *nth-1* germlines (data not shown) nor dysregulation of mitochondrial biogenesis genes in *nth-1* mutants [13]. Unlike NER, BER also functions in mitochondria, so it is possible that the mitochondrial dysfunction of *nth-1* mutants is a direct consequence of the mitochondrial DNA repair defect, although no mtDNA repair defect was observed following H_2O_2 treatment in *nth-1* [14]. Thus, the molecular mechanisms causing mitochondrial dysfunction in the *nth-1* mutant remains unknown, but it is possible that the *nth-1* mutants have a subtle mitochondrial DNA repair defect not detected by the qPCR assay or accumulation of mitochondrial mutations that affect mitochondrial function.

4.3. MAPK activation modulates response to paraquat

Previous gene expression profiling of *nth-1* mutants showed that genes involved in oxidative stress responses and innate immunity were differentially regulated in the *nth-1* mutant. Gene set enrichment analyses suggested that several genes known to be regulated by p38 MAPK and JNK stress-activated protein kinases were upregulated [13]. Here we present further experimental support for this observation: Using immunohistochemistry and western blot analyses we showed that *nth-1* mutants have elevated basal activation of PMK-1 and JNK-1, where JNK-1 phosphorylation was prominent in the germline.

Increased basal phosphorylation of JNK-1 and PMK-1 is consistent with constitutive SKN-1 activation [13] and upregulation of antioxidant defence genes such as *gst-4* and *sod-3* (Fig. 2D, E). A higher induction of CEP-1 dependent apoptotic corpses by ENU treatment is further supporting elevated MAPK kinase activation [39]. The basal MAPK activation is likely part of a complex compensatory transcriptional program that fine-tune cellular communication to compensate for NTH-1 deficiency. Because several MAPK, including PMK-1 [25] and JNK-1 (Supplementary Fig. S4E), are required for induction of apoptosis in response to paraquat, depletion of JNK-1 and PMK-1 expression by RNAi was not able to reactivate apoptosis competency in the *nth-1* mutant (Supplementary Fig. S4E).

However, we previously showed that oxidative stress response activation and transcriptomic reprogramming, or re-wiring, of *nth-1* mutants depended on XPA-1 [13] and vice versa, NTH-1 was required for compensatory transcriptome and proteome re-wiring of *xpa-1 mutants* [31]. Our current data is supportive of our previous observation and suggests that there might be collaboration between BER and NER at the damage recognition step. The mechanism behind activation of compensatory oxidative stress response in the *nth-1* mutant remains unknown but it is possible that the mild mitochondrial dysfunction and increased ROS production is sufficient for MAPK activation: Recently, it was shown that ROS, generated as a result of mitochondrial dysfunction, signalled through the apoptotic pathway to elicit a prolongevity response and that this ROS signal suppressed the longevity induced by paraquat and the mitochondrial respiratory chain mutant *isp-1* [40]. This would be consistent with a model in which the ROS signal generated through mild mitochondrial dysfunction elicits the compensatory stress response underlying the weak apoptotic response to paraquat. Interestingly, it was found that depletion of *nth-1* suppressed the increased lifespan of *isp-1* [40], which again would support a mechanism wherein mitochondrial dysfunction in *nth-1* mutants generates a ROS signal.

Alternatively, activation of MAPK could result from a systemic response to the presence of nuclear DNA damage in germ cells [41]. This is supported by the fact that depletion of XPA-1 and XPC-1, which function in nuclear but not mitochondrial DNA repair, suppresses basal JNK-1 activation.

Consistent with our interpretation that the attenuation of paraquat-induced apoptosis was a consequence of the compensatory stress response, we found that elevated basal phosphorylation of JNK-1, which was constitutively activated in the *nth-1* germline, correlated with the inability to activate apoptosis in response to paraquat. However, there was no indication that the degree of JNK-1 phosphorylation in paraquat-treated animals *per se* correlated with apoptosis induction, as JNK-1 phosphorylation was not induced in apoptosis competent *nth-1* mutants depleted for the NER proteins XPA-1 and XPC-1 (Fig. 5B and C).

Classical markers of DNA damage response activation such as RAD-51 foci (Supplementary Fig. S6) and transcriptional activation of the CEP-1 target gene *egl-1* (Fig. 3B and Supplementary Fig. S4B) were not induced in response to paraquat in wild type nor in the *nth-1* mutant. The failure of *nth-1* mutant to induce apoptosis is therefore unlikely to reflect a requirement for NTH-1-mediated processing of DNA damage to activate classical DNA damage signalling. Consistently, there was no activation of *egl-1* expression in *nth-1* mutants depleted for XPA-1, XPC-1, and CSB-1 excluding the possibility that apoptotic competency was gained because of a switch toward utilisation of classical DNA damage response signalling and CEP-1 dependent apoptosis (Supplementary Fig. S4B). Basal activation of MPK-1, a MAPK that regulates CEP-1 dependent apoptosis in the *C. elegans* germline [39], was not elevated in *nth-1* and it responded as strongly, or even much stronger, to paraquat as in the wild type (Supplementary Fig. S5).

In conclusion, we have demonstrated that *C. elegans nth-1* mutants exhibit a mild mitochondrial dysfunction phenotype and experience chronic oxidative stress. Their elevated ROS levels likely lead to altered bioenergetics and elevated basal MAPK activation that leads to an attenuated apoptotic responses to paraquat. These results show that a DNA repair mutant phenotype that could be interpreted as direct a consequence of the repair defect is more likely an indirect consequence of cytoprotective responses that compensate for DNA repair deficiency.

Conflict of interest

The authors declare that there is no conflict of interest.

Acknowledgements

The work was funded by grants from the FUGE (HKS, KDA, HN) programs at the Norwegian Research Council. HK was funded by the University of Oslo, and a grant (Project number 275911) from the South Eastern Norway Regional Health Authority. HKS was the recipient of a COST action Cangenin STSM grant. SE and NLB were supported by National Institutes of Health (R01 GM087628) and National Science Foundation (MCB-1330427) grants to SE).We thank Joanna Proszek, recipient for an ERASMUS training fellowship, for help with optimizing conditions for NTH-1 overexpression and purification and Magnar Bjørås for providing *E. coli* BK2118 and helpful discussion. HN and NV are members of the COST action GENiE.

Appendix A. Supplementary data

Supplementary data associated with this article can be found, in the online version, at https://doi.org/10.1016/j.dnarep.2017.11.009.

References

[1] I. Talhaoui, et al., Aberrant base excision repair pathway of oxidatively damaged DNA:implications for degenerative diseases, Free Radic. Biol. Med. 107 (2017) 266–277.
[2] M. Bosshard, E. Markkanen, B. van Loon, Base excision repair in physiology and pathology of the central nervous system, Int. J. Mol. Sci. 13 (12) (2012) 16172–16222.
[3] L. Stergiou, M.O. Hengartner, Death and more. DNA damage response pathways in the nematode C. elegans, Cell Death Differ. 11 (1) (2004) 21–28.
[4] N. Nakamura, et al., Cloning and characterization of uracil-DNA glycosylase and the biological consequences of the loss of its function in the nematode Caenorhabditis elegans, Mutagenesis 23 (5) (2008) 407–413.
[5] H.K. Skjeldam, et al., Loss of Caenorhabditis elegans UNG-1 uracil-DNA glycosylase affects apoptosis in response to DNA damaging agents, DNA Repair (Amst) 9 (8) (2010) 861–870.
[6] T. SenGupta, et al., Base excision repair AP endonucleases and mismatch repair act together to induce checkpoint-mediated autophagy, Nat. Commun. 4 (2013) 2674.
[7] H. Morinaga, et al., Purification and characterization of Caenorhabditis elegans NTH, a homolog of human endonuclease III: essential role of N-terminal region, DNA Repair (Amst) 8 (7) (2009) 844–851.
[8] A. Shatilla, et al., Characterization of Caenorhabditis elegans exonuclease-3 and evidence that a Mg2+-dependent variant exhibits a distinct mode of action on damaged DNA, Biochemistry 44 (38) (2005) 12835–12848.
[9] C. Zakaria, et al., Caenorhabditis elegans APN-1 plays a vital role in maintaining genome stability, DNA Repair (Amst) 9 (2) (2010) 169–176.
[10] Y. Kato, et al., Caenorhabditis elegans EXO-3 contributes to longevity and reproduction: differential roles in somatic cells and germ cells, Mutat. Res. 772 (2015) 46–54.
[11] A. Shatilla, D. Ramotar, Embryonic extracts derived from the nematode Caenorhabditis elegans remove uracil from DNA by the sequential action of uracil-DNA glycosylase and AP (apurinic/apyrimidinic) endonuclease, Biochem. J 365 (Pt 2) (2002) 547–553.
[12] K. Asagoshi, et al., Single-nucleotide base excision repair DNA polymerase activity in C: elegans in the absence of DNA polymerase beta, Nucleic Acids Res. 40 (2) (2012) 670–681.
[13] O.et al. Fensgard, A Two-tiered compensatory response to loss of DNA repair modulates aging and stress response pathways, Aging (Albany NY) 2 (3) (2010) 26.
[14] S.E. Hunter, et al., In vivo repair of alkylating and oxidative DNA damage in the mitochondrial and nuclear genomes of wild-type and glycosylase-deficient Caenorhabditis elegans, DNA Repair (Amst) 11 (11) (2012) 857–863.
[15] S. Brenner, The genetics of Caenorhabditis elegans, Genetics 77 (1) (1974) 71–94.
[16] C.D. Link, et al., Direct observation of stress response in Caenorhabditis elegans using a reporter transgene, Cell Stress Chaperones 4 (4) (1999) 235–242.
[17] S. Estes, et al., Natural variation in life history and aging phenotypes is associated with mitochondrial DNA deletion frequency in Caenorhabditis briggsae, BMC Evol. Biol. 11 (2011) 11.
[18] K.A.et al. Hicks, In vivo quantification reveals extensive natural variation in mitochondrial form and function in Caenorhabditis briggsae, PLoS One 7 (8) (2012) e43837.
[19] K.A. Hicks, D.R. Denver, S. Estes, Natural variation in Caenorhabditis briggsae mitochondrial form and function suggests a novel model of organelle dynamics, Mitochondrion 13 (1) (2013) 44–51.
[20] M. Takao, et al., Mitochondrial targeting of human DNA glycosylases for repair of oxidative DNA damage, Nucleic Acids Res. 26 (12) (1998) 2917–2922.
[21] T.W. O'Rourke, et al., Mitochondrial dysfunction due to oxidative mitochondrial DNA damage is reduced through cooperative actions of diverse proteins, Mol. Cell. Biol. 22 (12) (2002) 4086–4093.
[22] I. Bratic, J. Hench, A. Trifunovic, Caenorhabditis elegans as a model system for mtDNA replication defects, Methods 51 (4) (2010) 437–443.
[23] S.K. Park, P.M. Tedesco, T.E. Johnson, Oxidative stress and longevity in Caenorhabditis elegans as mediated by SKN-1, Aging Cell 8 (3) (2009) 258–269.
[24] M. Seervi, D. Xue, Mitochondrial cell death pathways in caenorhabiditis elegans, Curr. Top. Dev. Biol. 114 (2015) 43–65.
[25] L.S. Salinas, E. Maldonado, R.E. Navarro, Stress-induced germ cell apoptosis by a p53 independent pathway in Caenorhabditis elegans, Cell Death Differ. 13 (12) (2006) 2129–2139.
[26] B. Schumacher, et al., The C: elegans homolog of the p53 tumor suppressor is required for DNA damage-induced apoptosis, Curr. Biol. 11 (21) (2001) 1722–1727.
[27] A. Aballay, et al., Caenorhabditis elegans innate immune response triggered by Salmonella enterica requires intact LPS and is mediated by a MAPK signaling pathway, Curr. Biol. 13 (1) (2003) 47–52.
[28] B. Pei, et al., Arsenite-induced germline apoptosis through a MAPK-dependent: p53-independent pathway in Caenorhabditis elegans, Chem. Res. Toxicol. 21 (8) (2008) 1530–1535.
[29] L.M. McNamee, M.H. Brodsky, p53-independent apoptosis limits DNA damage-induced aneuploidy, Genetics 182 (2) (2009) 423–435.
[30] M. Christmann, B. Kaina, Transcriptional regulation of human DNA repair genes following genotoxic stress: trigger mechanisms, inducible responses and genotoxic adaptation, Nucleic Acids Res. 41 (18) (2013) 8403–8420.
[31] K.D. Arczewska, et al., Active transcriptomic and proteomic reprogramming in the C: elegans nucleotide excision repair mutant xpa-1, Nucleic Acids Res. 41 (10) (2013) 5368–5381.
[32] H. Lans, W. Vermeulen, Nucleotide excision repair in caenorhabditis elegans, Mol. Biol. Int. 2011 (2011) 542795.
[33] J. Pothof, et al., Identification of genes that protect the C: elegans genome against mutations by genome-wide RNAi, Genes Dev. 17 (4) (2003) 443–448.
[34] D.R. Denver, et al., The relative roles of three DNA repair pathways in preventing Caenorhabditis elegans mutation accumulation, Genetics 174 (1) (2006) 57–65.
[35] A. Vazquez, et al., Catabolic efficiency of aerobic glycolysis: the Warburg effect revisited, BMC Syst. Biol. 4 (2010) 58.
[36] F. Fang Evandro, et al., Defective mitophagy in XPA via PARP-1 hyperactivation and NAD+/SIRT1 reduction, Cell 157 (4) (2014) 882–896.
[37] M. Scheibye-Knudsen, et al., Cockayne syndrome group A and B proteins converge on transcription-linked resolution of non-B DNA, Proc. Natl. Acad. Sci. U. S. A. 113 (44) (2016) 12502–12507.
[38] E.F. Fang, et al., Nuclear DNA damage signalling to mitochondria in ageing, Nat. Rev. Mol. Cell Biol. 17 (5) (2016) 308–321.
[39] R.et al. Rutkowski, Regulation of Caenorhabditis elegans p53/CEP-1-dependent germ cell apoptosis by Ras/MAPK signaling, PLoS Genet. 7 (8) (2011) e1002238.
[40] C. Yee, W. Yang, S. Hekimi, The intrinsic apoptosis pathway mediates the pro-longevity response to mitochondrial ROS in C elegans, Cell 157 (4) (2014) 897–909.
[41] M.A. Ermolaeva, et al., DNA damage in germ cells induces an innate immune response that triggers systemic stress resistance, Nature 501 (7467) (2013) 416–420.